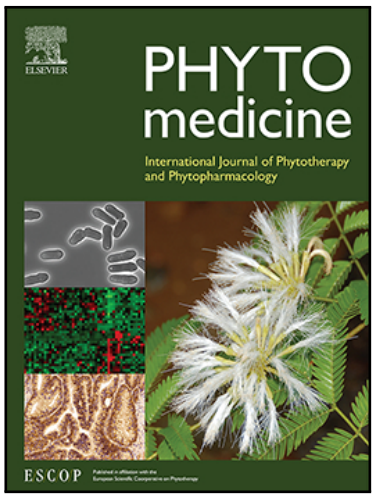

EGFR/MAPK signaling pathway acts as a potential therapeutic target for sulforaphane-rescued heart tube malformation induced by various concentrations of PhIP exposure

Guang Wang , Ran Zhao , Xinxia Zhang , Ying Zheng , Feiling Xie , Yu Jiang , Guohua Lv , Denglu Long , Chengyang Sun , Yongping Bao , Shuangyu Qi , Xinyue Liu , Qihao Zhang , Xuesong Yang

PII: S0944-7113(23)00628-1
DOI: https://doi.org/10.1016/j.phymed.2023.155270
Reference: PHYMED 155270

To appear in: *Phytomedicine*

Received date: 9 May 2023
Revised date: 14 November 2023
Accepted date: 7 December 2023

Please cite this article as: Guang Wang , Ran Zhao , Xinxia Zhang , Ying Zheng , Feiling Xie , Yu Jiang , Guohua Lv , Denglu Long , Chengyang Sun , Yongping Bao , Shuangyu Qi , Xinyue Liu , Qihao Zhang , Xuesong Yang , EGFR/MAPK signaling pathway acts as a potential therapeutic target for sulforaphane-rescued heart tube malformation induced by various concentrations of PhIP exposure, *Phytomedicine* (2023), doi: https://doi.org/10.1016/j.phymed.2023.155270

EGFR/MAPK signaling pathway acts as a potential therapeutic target for sulforaphane-rescued heart tube malformation induced by various concentrations of PhIP exposure

Guang Wang [1,2#*] , Ran Zhao [1#] , Xinxia Zhang [1#] , Ying Zheng[1#], Feiling Xie [1] ,Yu Jiang [1] , Guohua Lv [1] , Denglu Long [1] , Chengyang Sun[1], Yongping Bao [3] , Shuangyu Qi [1] , Xinyue Liu [1] , Qihao Zhang[4], Xuesong Yang [1,2, 5*]

[1] International Joint Laboratory for Embryonic Development & Prenatal Medicine, Division of Histology and Embryology, Medical College, Jinan University, Guangzhou 510632, China

[2] Key Laboratory for Regenerative Medicine of the Ministry of Education, Jinan University, Guangzhou 510632, China

[3] Norwich Medical School, University of East Anglia, Norwich, Norfolk NR4 7UQ, U.K.

[4] Department of Cell Biology & Institute of Biomedicine, College of Life Science and Technology, Jinan University, Guangzhou 510632, China

[5] Clinical Research Center, Clifford Hospital, Guangzhou 511495, China

[#] contributed to the work equally

*Corresponding authors: Xuesong Yang (Email: yang_xuesong@126.com, yangxuesong@jnu.edu.cn) (Tel:+86-20-85228316) or Guang Wang (Email: wangguang7453@126.com, t_wangguang@jnu.edu.cn) (Tel:+86-20-85220254)

Abstract

Background: 2-Amino-1-methyl-6-phenylimidazo [4,5-b] pyrimidine (PhIP) is a known carcinogen generated mainly from cooking meat and environmental pollutants. It is worth exploring the potential of natural small-molecule drugs to protect against adverse effects on embryonic development.

Purpose: In this study, we investigated the potential toxicological effects of PhIP on embryonic heart tube formation and the effect of SFN administration on the anti-toxicological effects of PhIP on embryonic cardiogenesis.

Study design and Methods: First, the chicken embryo model was used to investigate the different phenotypes of embryonic heart tubes induced by various concentrations of PhIP exposure. We also proved that SFN rescues PhIP-induced embryonic heart tube malformation. Second, immunofluorescence, western blot, Polymerase Chain Reaction (PCR) and flow cytometry experiments were employed to explore the mechanisms by which SFN protects cardiac cells from oxidative damage in the presence of PhIP. We used RNA-seq analysis, molecular docking, *in situ* hybridization, cellular thermal shift assay and solution nuclear magnetic resonance spectroscopy to explore whether SFN protects cardiogenesis through the EGFR/MAPK signaling pathway.

Results: The study showed that PhIP might dose-dependently interfere with the C-looping heart tube (mild) or the fusion of a pair of bilateral endocardial tubes (severe) in chick embryos, while SFN administration prevented cardiac cells from

oxidative damage in the presence of high-level PhIP. Furthermore, we found that excessive reactive oxygen species (ROS) production and subsequent apoptosis were not the principal mechanisms by which low-level PhIP induced malformation of heart tubes. This is due to PhIP-disturbed Mitogen-activated protein kinase (MAPK) signaling pathway could be corrected by SFN administration.

Conclusions: This study provided novel insight that PhIP exposure could increase the risk of abnormalities in early cardiogenesis and that SFN could partially rescue various concentrations of PhIP-induced abnormal heart tube formation by targeting EGFR and mediating EGFR/MAPK signaling pathways.

Keywords: PhIP; sulforaphane; heart tube formation; EGFR/MAPK signaling; oxidative stress; apoptosis

Abbreviations

ADT, AutoDock Tools; ATCC, American Type Culture Collection; BMP2, Bone morphogenetic protein 2; Bax, Bcl2 associated protein X; Bcl2, B-cell lymphoma-2; BW, Body weight; CCK-8, Cell Counting Kit-8; CETSA, Cellular Thermal Shift Assay; C-caspase3, Cleaved-caspase3; CRKL, CRK like proto-oncogene; CTSK, Cathepsin K; DAPI, 4',6-diamidino-2-phenylindole; DCF, 2',7'-dichlorodihydrofluorescein; DCFH-DA, 2',7'-dichlorodihydrofluorescein diacetate; DEGs, Differentially expressed genes; DHE, Dihydroethidium; DMSO, Dimethyl sulfoxide; DMSO-d6, Dimethyl sulfoxide-d6; D_2O, Deuteroxide; EGFR, Epidermal growth factor receptor; EC, Early chick; FBS, Fetal bovine serum; FGF, Fibroblast growth factor; FDR, False discovery rate; HRP, Horseradish Peroxidase; HO-1: Heme oxygenase; HH, Hamburger & Hamilton; KEGG, Kyoto Encyclopedia of Genes and Genomes; KRAS, Kirsten rat sarcoma viral oncogene; MAPK, Mitogen-activated protein kinase; MIF, Macrophage migration inhibitory factor; NKX2.5, NK2 homeobox 5; NMR, Nuclear Magnetic Resonance Spectroscopy; NOS2, Nitric oxide synthase 2; Nrf2, Nuclear factor erythroid-2-related factor 2; PBS, Phosphate buffered saline; PCR, Polymerase Chain Reaction; PDB, PBS protein data bank; PFA, Paraformaldehyde; PhIP, 2-Amino-1-methyl-6-phenylimidazo [4,5-b] pyrimidine; PI, Propidium iodide; PPI, Protein-protein interaction; QVina-W, QuickVina-W; ROS, Reactive oxygen species; SFN, Sulforaphane; SOD-1, Recombinant Superoxide Dismutase 1; SRA, Sequence Read Archive; Tbx20, T-box

transcription factor 20; TRPA1, Transient receptor potential cation channel subfamily A member 1; Vitamin C, VC.

Introduction

Embryonic/fetal development is a very complex process which includes a number of coordinated complex processes in physiological conditions (Zhu, 2016). The human heart is the first organ to form and function during embryogenesis (Buckingham et al., 2005). In terms of morphological alteration during embryonic heart development, it is chronologically composed of primary heart tube fusion, cardiac looping and accretion, cardiac septation and coronary vasculogenesis (Martinsen, 2005). Embryonic/fetal heart development is precisely and spatiotemporally regulated by a series of cardiac-specific gene expressions at different developmental stages. For instance, The well-documented transcription factors, NK2 homeobox 5(NKX2.5), GATA factors, myocardin and T-box transcription factor 20(Tbx20), are regarded to characterize and induce cardiogenic differentiation (Brand, 2003), so that they are often considered common cardiogenic factors (Martinsen, 2005). Mitogen-activated protein kinase are a well-known family of proteins that have an integral role on during cardiac development and physiological adaptation in mediating the cellular responses to various stimuli through complex and coordinated signaling events (Rose et al., 2010). The activation of Epidermal growth factor receptor (EGFR), which would cause the transactivation of mitogen-activated protein kinase (MAPK), is involved in regulating cell proliferation, apoptosis, migration, and differentiation (Fischer et al., 2006). Teratogen exposure, including medications, recreational drugs, tobacco, chemicals, alcohol, and infections during pregnancy, is a common cause of fetal abnormalities (Gilbert-Barness, 2010). (Jamkhande et al., 2014). However, an increasing number of teratogens are being discovered, and further exploration is required to understand how these new teratogens interfere with cardiac-specific gene expressions at different developmental stages.

Among the *identified* nineteen *heterocyclic amines*, 2-Amino-1-methyl-6-phenylimidazo [4,5-b] pyrimidine (PhIP) is the *most abundant and largely produced* during the process of *cooking* beef, pork and chicken meat (Keum et al., 2005; Wong et al., 2005). *PhIP* has been regarded as one of the important teratogenic factors, for example, it has been identified to be relevant in the malformation of the nervous system (Zhang et al., 2021). Traditionally, the toxicological effects of PhIP are embodied in causing damage of protein, lipid and DNA oxidative, as well as inducing carcinogenesis (Bellamri et al., 2018). Exposure to PhIP also increases the level of reactive oxygen species (ROS) in the body (Rose et al., 2010). PhIP derived from the external environment can be transfered to the fetus in a mother's womb via the placental barrier (Hasegawa et al., 1995; Myllynen et al., 2008). Thus, excessive PhIP exposure during pregnancy may directly influence on developing embryos and fetuses, thereby increasing the risk of embryonic/fetal developmental abnormality (Zhang et al., 2021). Due to the unavoidability of PhIP as a teratogenic factor, it is worth exploring the potential of natural small-molecule drugs to protect against adverse effects on embryonic development. However, at this stage, there is a lack of similar research.

Sulforaphane (SFN) is a dietary phytochemical, which belongs to isothiocyanate family and is derived from glucoraphanin from cruciferous vegetables (Kiser et al., 2021). SFN derived from food, dietary supplements or medicine has been realized and merely tolerated by humans (Fahey and Kensler, 2013; Fahey et al., 2012). As a potent indirect antioxidant, SFN could protect various cells (e.g., neurons, glial cells, microglia and astrocytes) from cellular injury induced by oxidative stress through reducing free radical production (Danilov et al., 2009; Greco and Fiskum, 2010; Negrette-Guzmán, 2019; Russo et al., 2018; Soriano et al., 2008). In the previous

studies, we found that SFN significantly rescued ethanol-suppressed angiogenesis and PhIP-induced early abnormal embryonic neurodevelopment in chick embryos (Wang et al., 2018b; Zhang et al., 2021). In this study, we firstly investigated the potential toxicological effects of PhIP on embryonic heart tube formation, and then focused on if/how SFN could rescue the PhIP-induced injury on early cardiogenesis.

Material and methods

Avian embryos and treatments

Fertilized chick eggs were acquired from the Avian Farm of the South China Agriculture University. The gastrula stage chick embryos were incubated in the early chick (EC) culture (Chapman et al., 2001) in a humidified incubator (Yiheng Instrument, Shanghai, China) at 38 °C and 70% humidity until the required HH stage (Hamburger and Hamilton, 1992). For the exposure of PhIP (Santa Cruz Biotechnology, CA, USA; 98%) and SFN (Sigma-Aldrich, MO, USA, 95%), HH0 chick embryos were incubated with EC culture mediums containing different concentrations of PhIP or SFN, while 0.1% DMSO (dimethyl sulfoxide, Sigma-Aldrich, MO, USA) were employed as control. For the Vitamin C (VC) − treated embryos, the HH4 chick embryos in EC culture were incubated with 2.86 mM VC (Beyotime Biotechnology Co., Shanghai, China; 99%) according to experimental requirements (Gao et al., 2018b). The afore-mentioned treated embryos were further incubated for the desired times according to the experimental requirement.

Cell culture and administration

H9c2 (rat cardiomyoblasts) cells (McElhinny et al., 2004) were obtained from

ATCC (American Type Culture Collection, CLR-1446, USA). The H9c2 cells were incubated in Dulbecco's modified Eagle's medium (DMEM/F12, Gibco, Shanghai, China) supplemented with 10% fetal bovine serum (FBS) (ExCell Bio, Shanghai, China) at 37 °C and 5% CO_2. For Cell Counting Kit-8 (CCK-8) assays, H9c2 cells were seeded into 96-well plates in the density of 1×10^4 cells/well. Following adherence, the cells were treated with various concentrations of PhIP (12.5, 25, 50, 100, 200 and 300 μM) or SFN (1, 5, 10 and 20 μM) alone, or 200 μM PhIP in the presence of several concentrations (1, 5 and 10 μM) of SFN or 40 μg/m VC (Gao et al., 2018b) for 12 h, 24 h, 36 h and 48 h, respectively. Control group was similarly treated in the absence of PhIP or SFN. After treatment, 10 μL aliquots of CCK-8 solution (GLPBIO, CA, USA) were added to each well and then incubated at 37 °C for 2 h. BIO-RAD Microplate Reader (Model 450, BIO-RAD, CA, USA) was used to detect optical density of the viable cells at 450 nm. Each treatment was implemented in triplicate.

Immunofluorescent, TUNEL and Hoechst/PI staining

Whole-mount embryo or cell immunostaining was performed as previously described (Wang et al., 2018b). Briefly, chick embryos or H9c2 cells were fixed in 4% Paraformaldehyde (PFA) (Sigma-Aldrich, MO, USA) overnight at 4 °C and then incubated in a solution containing the following primary antibodies: MF-20 (1:500, DSHB, IA, USA), γ-H2AX (1:200, DSHB, IA, USA), cleaved-caspase3(c-caspase3) (1:200, DSHB, IA, USA), PH3 (1:200, DSHB, IA, USA), Nuclear factor erythroid-2-related factor 2 (Nrf2) (1:200, Proteintech, 16396-1-AP) overnight at 4 °C. The anti-mouse or/and anti-rabbit IgG conjugated to Alexa Fluor 555/488 (abcam, Cambridge, UK) were chosen according to the primary antibodies and further

incubated with the embryos overnight at 4 °C on a rocker. All the chick embryos or cells were later counterstained with 4',6-diamidino-2-phenylindole (DAPI) (1:1000, Invitrogen, CA, USA) at room temperature for 1-2 h. For Hoechst/propidium iodide (PI) staining, H9c2 cells were incubated for 24 h and then treated with or without 200 μM PhIP alone or in combination with 5 μM SFN for further 24 h. After treatment, cells were washed twice with phosphate buffered saline (PBS) (Genview, Beijing, China) and incubated with Hoechst/PI in the dark at 37 °C for 30 min. The TUNEL staining was performed with ApopTag fluorescein direct in situ apoptosis detection kit (Elabscience Biotechnology Co.,Ltd, Wuhan, China), according to manufacturer's instructions.

Western blot

Western blot experiments for identifying the proteins from either chick embryos or H9c2 cells were performed with at least three replicates as described previously (Wang et al., 2018b). Primary antibodies including Nrf2 (1:200, Proteintech, 16396-1-AP), B-cell lymphoma-2 (Bcl2) (1:1000, Cell Signaling Technology, 3498S), Bcl2 associated protein X (Bax) (1:1000, Cell Signaling Technology, 2772S), c-caspase3 (1:1000, Cell Signaling Technology, #9664), p44/42 MAPK (1:1000, Cell Signaling Technology, #4695), Phospho-p44/42 MAPK (1:1000, Cell Signaling Technology, #4370), EGFR (1:1000, Cell Signaling Technology, #4267), Phospho-EGFR (1:1000, Cell Signaling Technology, #3777), GATA4 (1:1000, Abcam, ab134057) were used to detect their expressions at protein level. The loading control was a β-actin antibody (1:1000, Abcam, ab32572, New Territories, HK). After incubation with the secondary antibodies, i.e., either Horseradish Peroxidase (HRP) goat anti-rabbit IgG (1:3000, EarthOx, 7074S, Millbrae, USA) or HRP goat

anti-mouse IgG (1:3000, EarthOx, 7076S, Millbrae, USA), the samples were developed with SuperSignalTM West Femto Chemiluminescent Substrate (ThermoFisher, Rockford, USA) and the Gel Doc™ XR+ System (Bio-Rad, CA, USA).

RNA isolation and quantitative PCR

Total RNA was extracted from either chick embryos or H9c2 cells using a TRIzol kit (Invitrogen, CA, USA). PCR amplification of the cDNA was implemented using the corresponding specific primers (note: the sequences are provided in **Table S1**). The PCR reactions were implemented in a Bio-Rad S1000TM Thermal cycler (Bio-Rad, CA, USA) as previously described (Song et al., 2020). The quantitative PCR result was a representative of at least three independent experiments.

Measurement of oxidative stress

Intracellular ROS was measured using a non-fluorescent dye 2',7'-dichlorodihydrofluorescein diacetate (DCFH-DA) (Sigma-Aldrich, MO, USA). Briefly, the H9c2 cells were administrated without or with 25 or 200 μM PhIP alone or in combination with several concentrations (1, 5 and 10 μM) of SFN for 24 h. After treatment, the H9c2 cells were collected to be stained with DCFH-DA based on the standard protocol (Wang et al., 2018b). Concisely, the H9c2 cells from control, PhIP alone, or PhIP + SFN groups were incubated with DCFH-DA (10 μM) in serum-free culture medium at 37°C for 20 min. 330 μL aliquots of samples were obtained from each group for measuring fluorescence of 2',7'-dichlorodihydrofluorescein (DCF) using flow cytometry (BD FACSCanto II, BD Biosciences, CA, USA). For dihydroethidium (DHE) (BestBio, Shanghai, China) staining, 5 μM DHE was added

into the H9c2 cells from control, PhIP alone, and PhIP + SFN groups, and then incubated in the dark at 37 °C for 30 min.

Determination of apoptotic cells

Annexin V-FITC (BD Bioscience, NJ, USA) and PI double-staining were employed to quantitively detect apoptotic cells as previously described (Wang et al., 2018b). Briefly, the pre-incubated H9c2 cells were administrated with or without 25 or 200 μM PhIP alone or in combination with 5 μM SFN for 24 h. After treatment, the H9c2 cells were collected and resuspended in cold PBS and then introduced into 200 μL aliquots of the Annexin V-binding buffer. After incubated with 2.5 μL aliquots of FITC-labeled Annexin V and 2.5 μL aliquots of PI in the dark at room temperature for 15 min, flow cytometery (BD FACSCanto II, BD Biosciences, CA, USA) was used to detect the labeled apoptotic cells.

Transcriptional profiling using RNA sequencing (RNA-seq)

Total RNA was extracted from control, PhIP-treated, and PhIP + SFN-treated HH10 chick embryos (N > 30 embryos in each group) using TRIzol® Reagent based on the manufacturer's instructions (Invitrogen). Genomic DNA was removed using DNase I (TaKara, Japan). RNA samples were delivered to Shanghai Majorbio Bio-Pharm Technology Co., Ltd (Shanghai, China) for sequencing analysis. Differentially expressed genes (DEGs) were identified with fold change ≥ 1.5 and false discovery rate (FDR) < 0.05 between control and PhIP-treated HH10 chicken embryos. Kyoto Encyclopedia of Genes and Genomes (KEGG) pathway analysis was conducted using the ClueGO plugin and Cytoscape software. RNA-seq raw data generated in this study have been deposited in the Sequence Read Archive (SRA)

database (accession code: PRJNA812345).

In situ hybridization

Whole-mount *in situ* hybridization of chick embryos was implemented based on a standard protocol of *in situ* hybridization (Henrique et al., 1995). All the probes were generated by PCR amplification and labeled probes were transcribed with the T7 polymerase and dioxigenin-UTP (Roche, Basel, Switzerland). Primer sequences are shown in **Table S2**. The stained whole-mount embryos were photographed by a stereomicroscope (Olympus MVX10, Tokyo, Japan), and then frozen sections were prepared on a cryostat microtome (LeicaCM1900, Wetzlar, Germany) at a thickness of 20 μm.

Drug-target interaction prediction

For target prediction, the SMILES of SFN (CID: 9577379) from PubChem (https://pubchem.ncbi.nlm.nih.gov/) was employed to visualize the structure and predict the target in the website of Swiss Target Prediction (http://www.swisstargetprediction.ch/).

Molecular docking

The crystal structure of EGFR (PDB: 7SZ5) was downloaded from the RSCB protein data bank (PDB) (http://www.rcsb.org/). Before molecular docking, open-source PyMOL (https://pymol.org) was employed to remove the non-standard amino acids, crystal water, and impurity chains from the primary structure of EGFR, which was acquired for further hydrogenation and recalculation. AutoDock Tools (ADT, version 4.2.6) was used to convert the protein into PDBQT format for use

(Morris et al., 2009). SFN (CID: 9577379) was obtained from PubChem and converted into PDB format through OpenBabel3.1.1 (O'Boyle et al., 2011). Energy minimization was performed by MMFF94 force field. Then, semi-flexible molecular docking studies were performed using QuickVina-W (QVina-W), which employs a specialized algorithm without limitations in search space size or number of residues for “blind docking” (Hassan et al., 2017). PyMOL and Discovery Studio visualizer were used to visualize the best conformation and analyze the interaction between EGFR and the small molecule compound SFN. Molecular docking calculations performed three times.

Ligand-observed assay using gradient spectroscopy (WaterLOGSY)

WaterLOGSY method (Dalvit et al., 2001; Dalvit et al., 2000) of solution NMR was used to confirm the protein-ligand binding (i.e., EGFR and SFN). Lyophilized recombinant human EGFR (25-645) was purchased from Sino Biological Inc. (China). Four samples were prepared for the experiment, including 280 μM SFN alone, 10 μM EGFR alone, the mixtures of 10 μM EGFR:140 μM SFN and 10 μM EGFR:280 μM SFN. All samples were dissolved in 1X PBS (pH 7.4) containing 8% deuteroxide (D_2O) and 0.25%-0.5% dimethyl sulfoxide-d6 (DMSO-d6). All WaterLOGSY spectra were recorded on Bruker Advance III HD 600-MHz spectrometer equipped with BBO BBF-H-D probe. The experiments were performed with a 180º inversion pulse applied over the water signal at ~4.7 ppm by means of a square shaped selective pulse of 2 ms. The mixing time of the experiment was set to 1.0 s. Each WaterLOGSY spectrum was acquired with 1024 scans and with a recovery delay of 2.0 s, and measured at temperature of 25 ºC. The WaterLOGSY spectra were analyzed by Bruker Topspin 3.2 (Bruker Biospin, Germany) before fourier transformation of the

data were multiplied with an exponential function with a line broadening of 2 Hz.

Cellular Thermal Shift Assay (CETSA)

Samples were prepared from both control (DMSO) and SFN-exposed cells (15 μM), and they were subsequently diluted with PBS, divided into aliquots. Following an incubation period of one hour at 37°C, lysates were heated for 3 minutes at various temperatures (37°C, 41°C, 45°C, 49°C, 53°C, 57°C, or 61°C), followed by a cooling period of 3 minutes at room temperature. The samples were then subjected to centrifugation at 12000 × g at 4°C for subsequent Western blotting analysis. The CETSA result was a representative of at least three independent experiments.

Protein-protein interaction (PPI) analysis

PPI network was administrated through imputing heart tube development-related potential candidate genes for the retrieval of interacting genes database (STRING) (https://cn.string-db.org/).

Data analysis

Statistical analysis was implemented using the SPSS 20.0 statistical package program. Construction of statistical charts was carried out using the GraphPad Prism 8 software package (GraphPad Software, CA, USA). The data were presented as average ± SD and were analyzed using ANOVA and Tukey's multiple comparisons test was employed to establish if there was any significant difference between the control and experimental data. $P < 0.05$ was deemed statistically significant.

Results

The exposure of PhIP increased the risk of abnormal development of embryonic heart tube

To systematically evaluate the correlation between PhIP exposure and the early cardiovascular developmental anomalies, a systemic review of the eligible literature available in PubMed was performed without the limitations on publication year or language of publication **(Fig. S1A)**. The results revealed that there were the associations between PhIP exposure and oxidative stress, cardiovascular disorders as well as congenital developmental defects although there was no direct evidence for PhIP causing cardiac dysplasia via oxidative stress **(Table S3)**. We then incubated gastrula chicken embryos with a range of concentrations of PhIP added to the EC culture medium **(Fig. 1A)**. Embryonic mortality increased in a dose-dependent manner when the PhIP-treated embryos were harvested at HH10 **(Fig. 1B)**. RNA-seq analysis revealed that the greatest differentially expressed genes in the PhIP-treated embryos were related to heart development **(Fig. S2 and Fig. 1C)**. Furthermore, MF20 immunofluorescence staining were performed in the gastrula chicken embryos, and showed that there were mild and severe abnormalities in the HH10 chicken embryos exposed to 200 μM PhIP **(Fig. 1D-D1)**. Taken together, these data clearly demonstrated that excessive exposure of PhIP could cause malformation of embryonic heart tubes, thereby increasing the probability of later cardiac dysplasia.

The administration of SFN could rescue PhIP-induced abnormal development of embryonic heart tube

Initially, SFN was chosen to fight with the abnormal embryonic heart tube induced by PhIP exposure since SFN has been regarded as an antioxidant (Wang et al.,

2018b), which was impressively verified by the systemic review about SFN antioxidant efficiency evidenced by SFN-related clinical studies obtained and screened from PubMed **(Fig. S1B, Table S4)**. To investigate the potential effects of SFN on PhIP-induced damage, the H9c2 cell viability were determined when exposed to 12.5-50 μM (Note: low-level PhIP did not changed cell vitality in 48 h), to 100-300 μM (Note: high-level PhIP inhibited cell vitality in 48 h) PhIP and SFN (1-20 μM) at different times **(Fig. 2A-B)**. The results showed the dose- and time-dependent characteristics of cell viability towards PhIP and SFN. In the subsequent rescue experiments, we found that the greatest effect was observed with 5 μM SFN on 200 μM PhIP-suppressed cell viability **(Fig. 2C)**.

Vitamin C (VC) was used as the positive control drug since it is a well-known an antioxidant compound and can help restore chick embryo normalcy and gene expression, which may have been disrupted by excessive reactive oxygen species (ROS) production induced by factors such as high salt, high glucose, etc (Gao et al., 2018b; Li et al., 2014; Wang et al., 2018a). The results indicated that the VC can promoted the cell viability especially in 12 hours under the PhIP treatment. However, the cell viability in the PhIP+VC group was significantly lower compared to the PhIP+5 μM groups.

Based on this concentration combination of PhIP and SFN, we carried out an experiment in gastrula chicken embryos. We observed that embryonic mortality and the development of embryos, including number of somites and embryo length, showed significant improvements after the addition of 5 μM SFN when compared to PhIP treatment. This improvement was not as pronounced with the addition of 1 μM SFN or VC (**Fig. S3 and Fig. 2D-F**). Furthermore, the rate of mild and severe heart tube abnormalities in HH10 chicken embryos exposed to 200 μM PhIP decreased after

the addition of 5 μM SFN (**Fig. 2G**). The MF20-labeled heart tube in the 200 μM PhIP + 5 μM SFN group exhibited similarities to the control group, and there was also a reduction in the number of γ-H2AX-labeled positive cells in the presence of PhIP (severe abnormalities) to some extent **(Fig. 2H-H1)**. All the above data suggests that SFN has the effect of rescuing PhIP-induced embryonic heart tube malformation.

Antioxidation acts as the principal mechanism of SFN-rescued abnormal development of embryonic heart tube induced by high-level PhIP exposure

A high concentration of PhIP (200 μM) treatment significantly increased the production of ROS in H9c2 cells, and addition of SFN significantly reversed the rise of ROS **(Fig. 3A)**. This result was confirmed by DHE-labelled ROS level in H9c2 cells, and this increased ROS could be suppressed by SFN in a dose-dependent manner **(Fig. 3B-B1)**. Meanwhile, Immunofluorescent staining and western blotting showed the suppression of Nrf2 expression by PhIP treatment, and this was significantly up-regulated again in the presence of 5 μM SFN **(Fig. 3C-D)**. Similarly, quantitative PCR demonstrated the same trends in the mRNA expression of both Nrf2 **(Fig. 3E)**, and its downstream target Recombinant Superoxide Dismutase 1 (SOD-1) **(Fig. 3F)**.

Excess ROS affected cell proliferation, as well as apoptosis and resulted in embryonic cardiovascular dysplasia (Gao et al., 2018a; Wang et al., 2015). In this study, addition of SFN could reverse 200 μM PhIP-induced apoptosis in H9c2 cells, as revealed by flow cytometry (Annexin V-FITC/PI) and Hoechst/PI staining **(Fig. 4A-B** and **Fig. S4A-B)**. Western blotting showed that 5μM SFN significantly down-regulated PhIP-enhanced expression of c-caspase3 **(Fig. 4C)**. Quantitative PCR manifested that SFN down-regulated the increased Bcl2 expression, up-regulated Bax

and PARP-1 expression induced by 200 μM PhIP at mRNA levels **(Fig. 4D-E and H)**. Western blotting confirmed the suppression of Bcl-2/Bax ratio induced by PhIP treatment, and this was significantly up-regulated again in the presence of 5 μM SFN (**Fig. 4F**). TUNEL staining confirmed the promotion of apoptosis by PhIP treatment, and this was significantly up-decreased again in the presence of 5 μM SFN (**Fig. 4G-G1**). Likewise, addition of 5 μM SFN could partially rescue MF20/c-caspase3 labelled split heart tubes (severe malformation) and decrease c-caspase3 positive cell numbers augmented by 200 μM PhIP **(Fig. 4I-I1)**. However, the c-caspase3 positive cell numbers did not significantly increased in the mild malformation heart tube. Meanwhile, SFN also improved PhIP-inhibited MF20/PH3 double immunolabeled-heart tubes and increased PH3 positive cell percentages **(Fig. S4C-C1)**. In summary, the evidence from the above experiment indicates that SFN indeed could reverse high-level PhIP-induced abnormal formation of embryonic heart tubes via an antioxidative role.

The effect of SFN upon low-level PhIP exposure-induced oxidative stress

There was no significant change on ROS level in H9c2 cells exposed to either low-level PhIP (25 μM) or various concentrations of SFN **(Fig. 5A)**, but quantitative PCR demonstrated that low-level PhIP significantly inhibited Nrf2, Heme oxygenase (HO-1), NAD(P)H:quinone oxidoreductase 1 (NQO-1), and SOD-1 mRNA expressions, which could be significantly reversed by 5 μM SFN **(Fig. 5B-E)**. Consistently, western blotting showed that low-level PhIP-suppressed Nrf2 expression was raised again following the treatment of 5 μM SFN **(Fig. 5F)**. However, neither low-level PhIP alone nor in combination with SFN affected the Bcl-2/Bax ratio **(Fig. 5G)**, which confirmed the apoptosis cell numbers were not significantly increased in

the mild malformation **(Fig. 4F)**. It is therefore speculated that there may be other mechanisms for SFN's counteraction on the low-level PhIP-induced negative effect on embryonic heart tube formation.

MAPK signaling might act as a key signaling pathway on SFN-reversed the above phenotypes induced by low-level PhIP

To determine the key signaling pathway involved in heart development, KEGG enrichment was employed for analyzing the data from control and PhIP-treated groups based on the DEGs, and the result revealed that the MAPK signaling pathway was impacted by PhIP exposure **(Fig. S2 and Fig. 6A)**. A heatmap displayed the dramatical reversal of PhIP-reduced expressions of MAPK signaling by the addition of SFN **(Fig. 6B)**. Ten hub genes were identified as having highly functional interconnection with MAPK1 in a module **(Fig. 6C)**. The subsequent verification experiment for those gene expressions in the absence or presence of low-level or high-level PhIP using quantitative PCR, which demonstrated that MAPK1, Caspase3, Kirsten rat sarcoma viral oncogene (KRAS), and CRK like proto-oncogene (CRKL) expressions were really associated with the treatments of PhIP alone or in combination with SFN **(Fig. 6D-E)**. Whole-mount MAKP1 *in situ* hybridization showed that SFN could rescue to some extent MAPK1 expressive inhibition in gastrula chicken embryos induced by PhIP **(Fig. 6F)**. Consistently, western blotting showed that PhIP-suppressed P-MAPK1/MAPK1 ratio were raised again following the treatment of 5 μM SFN in presence of both low-level and high-level PhIP **(Fig. 6G-H)**. However, P-MAPK3/MAPK3 ratio were raised again following the treatment of 5 μM SFN only in presence of low-level PhIP **(Fig. 6G-H)**, indicating the key role of MAPK1 signaling on SFN-rescued PhIP interference on heart tube formation.

SFN modulates MAPK signaling through specifically binding target EGFR molecule

To identify the potential targets of SFN, we drew the chemical structure of SFN **(Fig. 7A)** and predicted its target classes based on Swiss Target Prediction **(Fig. 7B)**, which indicated that 26.7% of the top 15 target belonged to the enzyme class. And the top 5 most probable protein targets of SFN were EGFR, Macrophage migration inhibitory factor (MIF), Nitric oxide synthase 2 (NOS2), Transient receptor potential cation channel subfamily A member 1 (TRPA1), and Cathepsin K (CTSK) **(Fig. 7C)**. Furthermore, molecule docking analysis showed that the binding energy for SFN and EGFR was -5.30 ± 0.27 kcal/mol, the pKi was 3.89 ± 0.20 μM. The three-dimension diagram displayed that SFN bound to amino acid residues in EGFR pocket, where SFN formed hydrogen bonds with Gln47, pi-Sulfur with Tyr45 and an attractive charge with Asp102 **(Fig. 7D)**. Based on NMR data for the detection of protein-ligand interactions, we performed a WaterLOGSY experiment and showed that SFN alone possesses the opposite sign **(Fig. 7E,** purple**)** from that of EGFR alone **(Fig. 7E,** green**)**, while SFN resonances in the mixtures of 10 μM EGFR:140 μM SFN and 10 μM EGFR:280 μM SFN possess the same sign to that of EGFR **(Fig. 7E,** red and blue**)**, e.g., ~2.63 ppm and ~1.79 ppm, indicating that SFN directly binds to EGFR. The interaction between SFN and EGFR was also verified by CETSA (**Fig. S5**). In the subsequent western blotting experiment, we showed that P-EGFR/EGFR ratio was inhibited by both high-level and low-level PhIP, and its ratio could be up-regulated again following the addition of SFN **(Fig. 7F-G)**, indicating the important role of EGFR/MAPK signaling pathway, i.e., SFN directly regulates by binding to EGFR in the process of rescuing PhIP-interfered heart tube formation **(Fig. 7H)**.

Next, String analysis clearly manifested that EGFR/MAPK signaling pathway was involved in the regulation of many well-known gene expressions in controlling cardiac development **(Fig. 8A)**. Whole-mount GATA5, VMHC, NK2 homeobox 5(NKX2.5) *in situ* hybridization showed that these cardiac-specific gene expressions in the side of PhIP-unilaterally treated chicken embryos were dramatically lower than control (opposite side) **(Fig. 8B-D)**. Western blotting **(Fig. 8E)** and quantitative PCR data (**Fig. 8F)** further revealed that 25 μM PhIP-inhibited expressions of cardiac-specific genes could be rescued by the addition of 5 μM SFN **(Fig. 8F)**. However, the blocking EGFR signaling with gefitinib (EGFR inhibitor) could reverse the improved effect of gene expression by SFN **(Fig. 8G)**. Interestingly, the ROS production inhibition by SFN against 200 μM PhIP was also weakened by gefitinib **(Fig. S6)**, indicating that activation of EGFR/MAPK signaling pathway is crucial for SFN to antagonize PhIP-damaged heart tube formation.

Discussion

Our systematic literature review indicated that PhIP exposure by pregnant women could directly endanger their fetuses, but that there were no reports of a detrimental effect by PhIP on early cardiogenesis **(Fig. S1 and Table S3)**. For the first time, we observed that PhIP could decrease H9c2 cell viability in a dose- and time-dependent manner and interfere with the C-looping heart tube (mild) or the fusion of a pair of bilateral endocardial tubes (severe) in this study **(Fig. 1-2)**. Although the PhIP exposure level is equivalent to a dose of 5.9 ng/kg body weight (BW) in human (Pouzou et al., 2018) and can be converted to a dose of 70 ng/kg BW for a mouse (Yang et al., 2021), but the dose of PhIP even at 200 mg/kg BW can also

be accepted for acute period in the mouse (Syeda et al., 2020). Furthermore, the PhIP concentrations used in H9c2 cells were also mimic with the PhIP induced cytotoxicity in breast epithelial cells (Jain et al., 2015). A range of 25-200 μM PhIP, which can be converted to a dose of 5.5-44 μg/kg, was employed in the chick embryo model, as this was also an acute toxicological experiment.

According to the cell viability data, effect of PhIP on early cardiogenesis could be divided into two groups: firstly, at PhIP concentrations less than 50 μM (low-level PhIP) and secondly, at PhIP concentrations greater than 100 μM (high-level PhIP; **Fig. 2**). It is probable that the mild and severe phenotypes of heart tube malformation may be attributed to the diversity of the cardiac progenitor cells in developing heart tube in presence of PhIP. In this study, the different phenotypes of heart tube malformations were presented when gastrula chicken embryos were treated with a uniform concentration of PhIP, and it could also be observed when they were exposed to low and high levels of PhIP. So, it can be speculated that the different phenotypes of malformation would correspond to the differently underlying pathological mechanisms. In addition, it suggests that PhIP induce injury to embryonic/fetal development is nonspecific since we previously found that the abnormal embryonic neurodevelopment was also induced by PhIP exposure (Zhang et al., 2021). The lack of a tissue-specific effect could be also observed in the bioinformatic analysis of RNA-seq data, in which there are many DEGs related to the development of nervous, urinary, and cardiovascular systems although the numbers are relatively low compared to the number of DEGs involved in heart development **(Fig. 1 and Fig. S2)**.

PhIP-induced DNA damage often occurs due to excessive ROS production in the presence of PhIP, and this was confirmed in high-level PhIP-treated H9c2 cells in this study **(Fig. 3)**. Appropriate concentrations of SFN (i.e., an antioxidant) were

employed to overcome the embryonic/fetal damage induced by PhIP exposure, and 5 μM SFN was shown to reverse the PhIP-induced reduction of H9c2 cell viability, as well as rescue to a degree PhIP-induced malformation of heart tube of chicken embryos **(Fig. 2 and Fig. S3)**. There wasn't a particularly suitable positive control drug for the protective effects on embryonic development, especially given the teratogenic nature of PhIP. We opted for the relatively safe antioxidant VC as our choice (Gao et al., 2018b; Li et al., 2014; Wang et al., 2018a). In this experiment, SFN exhibited a more pronounced rescuing effect on cell viability and embryonic heart tube development under PhIP exposure compared to VC. This could be attributed to SFN having multiple targets beyond its antioxidant properties. Consequently, in our subsequent experiments, we did not use VC as a positive control drug to evaluate the mechanism of action of SFN.

In the presence of SFN, a reduction of the elevated intracellular ROS level induced by high-level PhIP was detected and the inhibition of Nrf2 signaling induced by high-level PhIP was significantly restored **(Fig. 3)**. It appeared to further extend the antioxidative effect of SFN on preventing cardiac progenitor cells from oxidative damage when the developing embryos/fetuses are under conditions of oxidative stress. However, as the 10 μM SFN treatment was less effective in promoting cell viability than the 5 μM SFN treatment, this might due to the complex regulation of dose-dependent SFN on other signaling pathways (VEGF-VEGFR, etc.) (Bao et al., 2014; Liu et al., 2018; Wang et al., 2017). Further experimentation is required to investigate the precise molecular mechanisms involved. Based on the aforementioned data and our previous results (Wang et al., 2018b), the combination of 5 μM SFN with various concentrations of PhIP was administered together to reveal the underlying mechanisms.

Cellular redox changes, such as production of ROS, can partially involve the signal transduction pathway of apoptosis, i.e., ROS plays a crucial role in apoptotic processes (Kannan and Jain, 2000). In this study, a massive occurrence of cell apoptosis in both H9c2 cells and gastrula chick embryos was observed in the presence of high-level PhIP; SFN also reversed the expressions of key genes related to apoptosis, but could not completely rescue the malformation of heart tubes **(Fig. 4 and Fig. S4)**. Therefore, it is speculated that the aforementioned SFN-rescued effect on oxidative damage might occur in the high-level PhIP-induced malformation of heart tube, despite not demonstrating a complete recovery on the turbulence of early cardiogenesis. However, this raises another question as to whether low-level PhIP-induced cell damage was also due to excessive ROS-induced cell death in the developing embryos/fetuses, thereby interfering with heart tube formation normally. Determination of intracellular ROS levels in the presence of low-level PhIP showed no effects on ROS levels in such a case, and that there were no significant changes either following SFN addition, although Nrf2 expression was significantly repressed by PhIP and re-upregulated again by SFN. Correspondingly, low-level PhIP treatment did not cause a notable alteration of cell apoptosis **(Fig. 5)**. This fact confirms that excessive ROS production and subsequent apoptosis as discussed above might not be the principal mechanism for low-level PhIP to cause the malformation phenotype of heart tubes. If so, the rescuing effect by SFN could be additionally achieved via other mechanisms.

It is possible that low-level PhIP directly interferes with some crucial signaling pathways which are involved in regulating key gene expression in early cardiogenesis. There appear to be some cluesto solve this problem from the KEGG enrichment analysis of RNA-seq data, which indicated that the MAPK signaling pathway had the

most DEGs and this was verified by heatmap data and the network of the top 10 key genes most relevant to the MAPK pathway **(Fig. 6)**. Interestingly, not only low-level but also high-level PhIP-induced reduction of these key gene expressions could be rescued in most instances, suggesting that SFN-altered MAPK signaling activity might be associated with the effective mechanisms induced by low- or high-level PhIP. The next step is to determine by what mechanism SFN rescued the PhIP-induced abnormity of heart tube formation. Using Swiss Target Prediction, EGFR was predicted to be the most probable target of SFN. To determine the binding sites, we performed molecule docking and further identified that SFN directly interacts with EGFR through binding to the residues of domain I (e.g. Gln47, Tyr45, Asp102), which is proposed to be the domain that EGF binds to activate EGFR (Ogiso et al., 2002). Further, we used WaterLOGSY and CETSA to verify the direct binding between SFN and EGFR, indicated by the binding compound appearing with the same sign as the target protein (Dalvit et al., 2001; Dalvit et al., 2000). Western blot data also demonstrated that SFN could re-activate EGFR that is inactivated by PhIP, suggesting that SFN may act as an EGF-like ligand to activate EGFR **(Fig. 7 and Fig. S5)**. However, due to the estimated low binding affinity, mutant EGFR is required to further confirm the interaction between SFN and EGFR. EGFR, like many other growth-factor receptors, is situated the upstream of MAPK pathway, which triggers a series of phosphorylation-activating kinases, to complete the signaling transduction from cell surface to the nucleus (Koveitypour et al., 2019; Wee and Wang, 2017). Therefore, it is reasonable to presume that SFN's rescuing effect on PhIP-induced abnormality of heart tube formation was achieved by directly targeting the EGFR molecule and activating the EGFR/MAPK signaling pathway. In order to verify the speculation, we further applied an EGFR inhibitor, gefitinib, and

determined the expressions of EGFR/MAPK and key genes relevant to early cardiogenesis in absence or presence of PhIP and/or SFN, and the results demonstrated that the activity of EGFR/MAPK signaling was associated with the normal expressions of the crucial genes related to early cardiogenesis, as well as to the reversion of these gene expressions and ROS production by SFN **(Fig. 8 and Fig. S6)**.

In summary **(Fig. 9)**, a certain concentration of SFN application could rescue to some extent PhIP-induced heart tube phenotypes and H9c2 cell viability induced by dose- and time-dependent PhIP exposure. In addition to the antioxidant effects, we found that SFN could specifically bind to EGFR, which further confirmed that SFN was involved in regulating the expressions of key genes relevant to early cardiogenesis via EGFR/MAPK signaling pathway. Comprehensive evidence is offered for the first time that SFN can rescue various concentrations of PhIP-induced abnormal heart tube formation through targeting EGFR and mediating EGFR/MAPK signaling pathways. The range of applications for SFN has been expanded, which provides the possibility of further developing new ways for protecting embryo development from the impact of teratogeny induced by teratogens, such as PhIP derived from well-cooked meat foods.

Compliance with Ethics Requirements

All processes involving animal treatments in this study were in accordance with the procedures of Ethical Committee for Animal Experimentation (Approval No. IACUC-20181126-02, the ethical approval to perform animal experiments is from May. 7th, 2021), Jinan University.

Conflict of interests

The authors declare that they have no known competing financial interests or personal relationships that could have appeared to influence the work reported in this paper.

Contributors

Ran Zhao, Xinxia Zhang, Ying Zheng, Yu Jiang, Guohua Lv, Shuangyu Qi, and Xingyue Liu: Validation; Guang Wang, Ran Zhao, Xinxia Zhang, Ying Zheng, Feiling Xie: Formal analysis, Writing - Original Draft; Yongping Bao, Qihao Zhang: Writing - Review & Editing, Guang Wang and Xuesong Yang: Conceptualization, Methodology, Writing - Review & Editing, Supervision, Project administration, Funding acquisition. All data were generated in-house, and no paper mill was used. All authors agree to be accountable for all aspects of work ensuring integrity and accuracy.

Acknowledgements

This study was supported by National Natural Science Foundation of China [grant number 32170825, 31971108, 82371692]; the Science and Technology Program of Guangzhou [grant number 202201020007]; Guangdong Basic and Applied Basic Research Foundation [grant number 2023A1515010424]; the Fundamental Research Funds for the Central Universities [grant number 21621106]; Special Funds for the Cultivation of Guangdong College Students' Scientific and Technological Innovation [grant number pdjh2023b0065]. We would like to thank Medical experimental center

in Jinan University. We would like to thank Mr. Bai Wu (Qianshishe Animation Co., Ltd., Jinan, China) for drawing the summary figure.

References

Bao, Y., Wang, W., Zhou, Z., Sun, C., 2014. Benefits and risks of the hormetic effects of dietary isothiocyanates on cancer prevention. PLoS One 9, e114764.

Bellamri, M., Wang, Y., Yonemori, K., White, K.K., Wilkens, L.R., Le Marchand, L., Turesky, R.J., 2018. Biomonitoring an albumin adduct of the cooked meat carcinogen 2-amino-1-methyl-6-phenylimidazo [4, 5-b] pyridine in humans. Carcinogenesis 39, 1455-1462.

Brand, T., 2003. Heart development: molecular insights into cardiac specification and early morphogenesis. Dev. Biol. 258, 1-19.

Buckingham, M., Meilhac, S., Zaffran, S., 2005. Building the mammalian heart from two sources of myocardial cells. Nat. Rev. Genet. 6, 826-835.

Chapman, S.C., Collignon, J., Schoenwolf, G.C., Lumsden, A., 2001. Improved method for chick whole-embryo culture using a filter paper carrier. Dev. Dyn. 220, 284-289.

Dalvit, C., Fogliatto, G., Stewart, A., Veronesi, M., Stockman, B., 2001. WaterLOGSY as a method for primary NMR screening: practical aspects and range of applicability. J. Biomol. NMR 21, 349-359.

Dalvit, C., Pevarello, P., Tato, M., Veronesi, M., Vulpetti, A., Sundstrom, M., 2000. Identification of compounds with binding affinity to proteins via magnetization transfer from bulk water. J. Biomol. NMR 18, 65-68.

Danilov, C.A., Chandrasekaran, K., Racz, J., Soane, L., Zielke, C., Fiskum, G., 2009.

Sulforaphane protects astrocytes against oxidative stress and delayed death caused by oxygen and glucose deprivation. Glia 57, 645-656.

Fahey, J.W., Kensler, T.W., 2013. Health span extension through green chemoprevention. Am. J. Ethics Med. 15, 311-318.

Fahey, J.W., Talalay, P., Kensler, T.W., 2012. Notes from the field:"Green" chemoprevention as frugal medicine. Cancer Prev. Res. 5, 179-188.

Fischer, O.M., Hart, S., Ullrich, A., 2006. Dissecting the epidermal growth factor receptor signal transactivation pathway. Methods Mol. Biol. 327, 85-97.

Gao, L.R., Wang, G., Zhang, J., Li, S., Chuai, M., Bao, Y., Hocher, B., Yang, X., 2018a. High salt-induced excess reactive oxygen species production resulted in heart tube malformation during gastrulation. J. Cell. Physiol. 233, 7120-7133.

Gao, L.R., Wang, G., Zhang, J., Li, S., Chuai, M., Bao, Y., Hocher, B., Yang, X., 2018b. High salt-induced excess reactive oxygen species production resulted in heart tube malformation during gastrulation. J Cell Physiol 233, 7120-7133.

Gilbert-Barness, E., 2010. Review: Teratogenic Causes of Malformations. Ann. Clin. Lab. Sci. 40, 99-114.

Greco, T., Fiskum, G., 2010. Brain mitochondria from rats treated with sulforaphane are resistant to redox-regulated permeability transition. J. Bioenerg. Biomembr. 42, 491-497.

Hamburger, V., Hamilton, H.L., 1992. A series of normal stages in the development of the chick embryo. 1951. Dev. Dyn. 195, 231-272.

Hasegawa, R., Kimura, J., Yaono, M., Takahashi, S., Kato, T., Futakuchi, M., Fukutake, M., Fukutome, K., Wakabayashi, K., Sugimura, T., et al., 1995. Increased risk of mammary carcinoma development following transplacental and trans-breast milk exposure to a food-derived carcinogen, 2-amino-1-methyl-6-phenylimidazo[4,5-b]pyridine (PhIP), in Sprague-Dawley rats. Cancer Res. 55, 4333-4338.

Hassan, N.M., Alhossary, A.A., Mu, Y., Kwoh, C.K., 2017. Protein-Ligand Blind Docking Using QuickVina-W With Inter-Process Spatio-Temporal Integration. Sci. Rep. 7, 15451.

Henrique, D., Adam, J., Myat, A., Chitnis, A., Lewis, J., Ish-Horowicz, D., 1995. Expression of a Delta homologue in prospective neurons in the chick. Nature 375, 787-790.

Jain, A., Samykutty, A., Jackson, C., Browning, D., Bollag, W.B., Thangaraju, M., Takahashi, S., Singh, S.R., 2015. Curcumin inhibits PhIP induced cytotoxicity in breast epithelial cells through multiple molecular targets. Cancer Lett. 365, 122-131.

Jamkhande, P.G., Chintawar, K.D., Chandak, P.G., 2014. Teratogenicity: a mechanism based short review on common teratogenic agents. Asian Pac. J. Trop. Dis. 4, 421-432.

Kannan, K., Jain, S.K., 2000. Oxidative stress and apoptosis. Pathophysiology 7, 153-163.

Keum, Y.-S., Jeong, W.-S., Kong, A., 2005. Chemopreventive functions of isothiocyanates. Drug News Perspect. 18, 445-451.

Kiser, C., Gonul, C.P., Olcum, M., Genc, S., 2021. Inhibitory effects of sulforaphane on NLRP3 inflammasome activation. Mol. Immunol. 140, 175-185.

Koveitypour, Z., Panahi, F., Vakilian, M., Peymani, M., Forootan, F.S., Esfahani, M.H.N., Ghaedi, K., 2019. Signaling pathways involved in colorectal cancer progression. Cell Biosci. 9, 1-14.

Li, Y., Wang, X.Y., Zhang, Z.L., Cheng, X., Li, X.D., Chuai, M., Lee, K.K., Kurihara, H., Yang, X., 2014. Excess ROS induced by AAPH causes myocardial hypertrophy in the developing chick embryo. Int J Cardiol 176, 62-73.

Liu, P., Wang, W., Zhou, Z., Smith, A.J.O., Bowater, R.P., Wormstone, I.M., Chen, Y., Bao, Y., 2018. Chemopreventive Activities of Sulforaphane and Its Metabolites in Human Hepatoma HepG2 Cells. Nutrients 10.

Martinsen, B.J., 2005. Reference guide to the stages of chick heart embryology. Dev. Dyn. 233, 1217-1237.

McElhinny, A.S., Perry, C.N., Witt, C.C., Labeit, S., Gregorio, C.C., 2004. Muscle-specific RING finger-2 (MURF-2) is important for microtubule, intermediate filament and sarcomeric M-line maintenance in striated muscle development. J. Cell Sci. 117, 3175-3188.

Morris, G.M., Huey, R., Lindstrom, W., Sanner, M.F., Belew, R.K., Goodsell, D.S., Olson, A.J., 2009. AutoDock4 and AutoDockTools4: Automated docking with

selective receptor flexibility. J. Comput. Chem. 30, 2785-2791.

Myllynen, P., Kummu, M., Kangas, T., Ilves, M., Immonen, E., Rysa, J., Pirila, R., Lastumaki, A., Vahakangas, K.H., 2008. ABCG2/BCRP decreases the transfer of a food-born chemical carcinogen, 2-amino-1-methyl-6-phenylimidazo[4,5-b]pyridine (PhIP) in perfused term human placenta. Toxicol. Appl. Pharmacol. 232, 210-217.

Negrette-Guzmán, M., 2019. Combinations of the antioxidants sulforaphane or curcumin and the conventional antineoplastics cisplatin or doxorubicin as prospects for anticancer chemotherapy. Eur. J. Pharmacol. 859, 172513.

O'Boyle, N.M., Banck, M., James, C.A., Morley, C., Vandermeersch, T., Hutchison, G.R., 2011. Open Babel: An open chemical toolbox. J. Cheminform. 3, 33.

Ogiso, H., Ishitani, R., Nureki, O., Fukai, S., Yamanaka, M., Kim, J.H., Saito, K., Sakamoto, A., Inoue, M., Shirouzu, M., Yokoyama, S., 2002. Crystal structure of the complex of human epidermal growth factor and receptor extracellular domains. Cell 110, 775-787.

Pouzou, J.G., Costard, S., Zagmutt, F.J., 2018. Probabilistic assessment of dietary exposure to heterocyclic amines and polycyclic aromatic hydrocarbons from consumption of meats and breads in the United States. Food Chem. Toxicol. 114, 361-374.

Rose, B.A., Force, T., Wang, Y., 2010. Mitogen-activated protein kinase signaling in the heart: angels versus demons in a heart-breaking tale. Physiol. Rev. 90,

1507-1546.

Russo, M., Spagnuolo, C., Russo, G.L., Skalicka-Woźniak, K., Daglia, M., Sobarzo-Sánchez, E., Nabavi, S.F., Nabavi, S.M., 2018. Nrf2 targeting by sulforaphane: A potential therapy for cancer treatment. Crit. Rev. Food Sci. Nutr. 58, 1391-1405.

Song, J., Wang, C., Long, D., Li, Z., You, L., Brand-Saberi, B., Wang, G., Yang, X., 2020. Dysbacteriosis-induced LPS elevation disturbs the development of muscle progenitor cells by interfering with retinoic acid signaling. FASEB J. 34, 6837-6853.

Soriano, F.X., Léveillé, F., Papadia, S., Higgins, L.G., Varley, J., Baxter, P., Hayes, J.D., Hardingham, G.E., 2008. Induction of sulfiredoxin expression and reduction of peroxiredoxin hyperoxidation by the neuroprotective Nrf2 activator 3H-1, 2-dithiole-3-thione. J. Neurochem. 107, 533-543.

Syeda, T., Foguth, R.M., Llewellyn, E., Cannon, J.R., 2020. PhIP exposure in rodents produces neuropathology potentially relevant to Alzheimer's disease. Toxicology 437, 152436.

Wang, G., Huang, W.Q., Cui, S.D., Li, S., Wang, X.Y., Li, Y., Chuai, M., Cao, L., Li, J.C., Lu, D.X., Yang, X., 2015. Autophagy is involved in high glucose-induced heart tube malformation. Cell Cycle 14, 772-783.

Wang, G., Liang, J., Gao, L.R., Si, Z.P., Zhang, X.T., Liang, G., Yan, Y., Li, K., Cheng, X., Bao, Y., Chuai, M., Chen, L.G., Lu, D.X., Yang, X., 2018a. Baicalin

administration attenuates hyperglycemia-induced malformation of cardiovascular system. Cell Death Dis 9, 234.

Wang, G., Nie, J.-h., Bao, Y., Yang, X., 2018b. Sulforaphane rescues ethanol-suppressed angiogenesis through oxidative and endoplasmic reticulum stress in chick embryos. J. Agric. Food. Chem. 66, 9522-9533.

Wang, Y., Zhou, Z., Wang, W., Liu, M., Bao, Y., 2017. Differential effects of sulforaphane in regulation of angiogenesis in a co-culture model of endothelial cells and pericytes. Oncol. Rep. 37, 2905-2912.

Wee, P., Wang, Z., 2017. Epidermal growth factor receptor cell proliferation signaling pathways. Cancers (Basel) 9, 52.

Wong, K.-Y., Su, J., Knize, M.G., Koh, W.-P., Seow, A., 2005. Dietary exposure to heterocyclic amines in a Chinese population. Nutr. Cancer 52, 147-155.

Yang, X., Peng, H., Luo, Z., Luo, A., Cai, M., Xu, L., Wang, H., 2021. The dietary carcinogen PhIP activates p53-dependent DNA damage response in the colon of CYP1A-humanized mice. BioFactors 47, 612-626.

Zhang, P., Li, T., Liu, C., Sindi, M., Cheng, X., Qi, S., Liu, X., Yan, Y., Bao, Y., Brand-Saberi, B., 2021. Nano-sulforaphane attenuates PhIP-induced early abnormal embryonic neuro-development. Ann. Anat. 233, 151617.

Zhu, H., 2016. Forkhead box transcription factors in embryonic heart development and congenital heart disease. Life Sci. 144, 194-201.

Figure legends

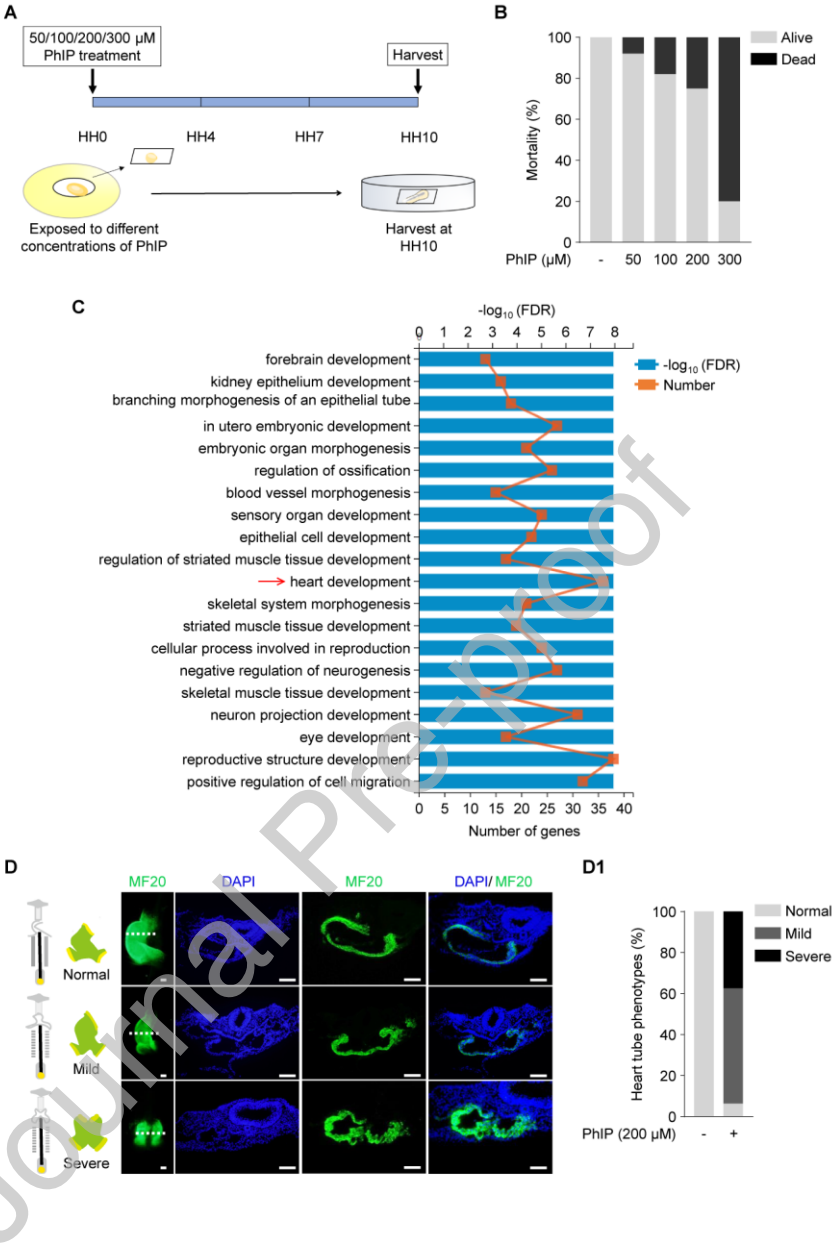

Fig. 1. Assessing the effect of PhIP exposure on the early development of heart.

(**A**) Schematic illustration of PhIP exposure to gastrula chicken embryos and the harvest time. (**B**) Bar chart showing the embryonic mortality when exposed to various concentrations of PhIP. (**C**) Bioinformatic analysis of RNA-seq data from DMSO-treated and 200 μM PhIP-treated groups displaying the gene numbers of differentially expressed genes (DEGs) related to the developments of different

systems. (**D**-**D1**) Representative images of heart tubes (MF20 immunofluorescent staining) of gastrula chicken embryos after 200 μM PhIP treatment, as well as the cross sections of heart tubes at the leveled indicated by white dotted lines (**D**). Bar chart showing the percentages of hear tube phenotypes (normal, mild and severe) (**D1**). Data were mean ± SD. n = 100 (**A**), or n = 3 (**D**). Scale bars = 50 μm in **D**.

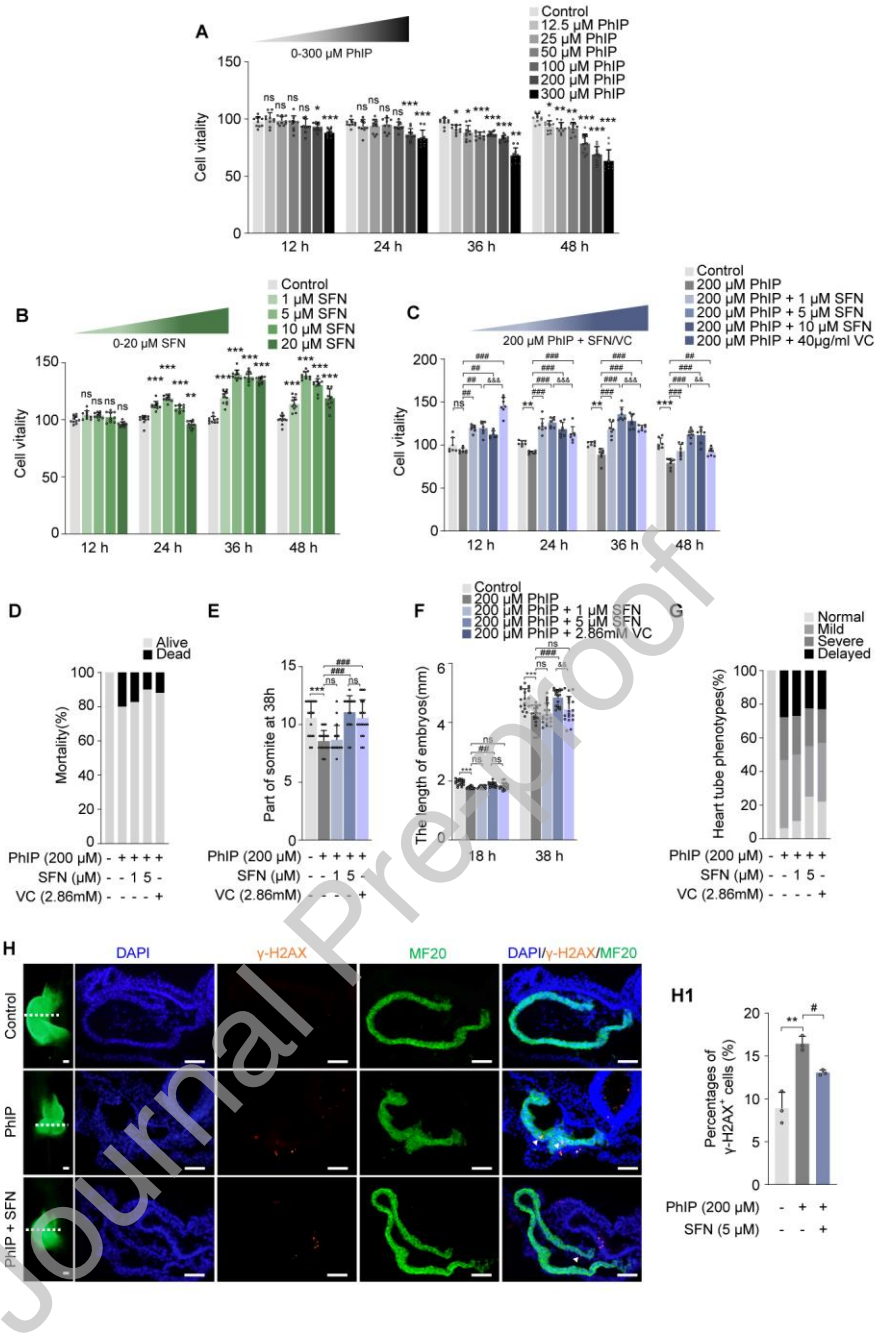

Fig. 2. Assessing the effect of SFN and VC on the decrease in H9c2 cell viability and the abnormal development of heart tubes induced by PhIP. (**A-C**) The bar charts show the comparisons of H9c2 cell viability when exposed to various concentrations of PhIP (0, 12.5, 25, 50, 100, 200 and 300 μM) (**A**), SFN (0, 1, 5, 10 and 20 μM) (**B**), 200 μM PhIP in the presence of various concentrations of SFN (0, 1, 5 and 10 μM) and VC (40μg/ml) (**C**) for 12 h, 24 h, 36 h and 48 h. (**D-F**) Bar chart

showing comparisons of chick embryo's the mortality **(D)**, pairs of somites **(E)** and lengths of embryos **(F)** among control, 200 μM PhIP alone, 200 μM PhIP + 1 μM SFN groups, 200 μM PhIP + 5 μM SFN groups, and 200 μM PhIP + 2.86mM VC groups at 18h or 38h. (**G**) Bar chart showing the percentages of hear tube phenotypes (normal, mild, severe and delayed) at HH10. (**H-H1**) Representative images of gastrula chicken embryo heart tubes (MF20 or γ-H2AX immunofluorescent staining) from control, 200 μM PhIP alone, and 200 μM PhIP + 5 μM SFN groups, as well as the cross sections of heart tubes at the level indicated by white dotted lines (**H**). Bar chart showing the percentages of γ-H2AX positive cells from the above-mentioned groups (**H1**). Data were mean ± SD. n =10 (**A**, **B**), n=7(**C**), n = 18 (**D**-**G**), or n=3(**H**). $^{*}P < 0.05$, $^{**}P < 0.01$, $^{***}P < 0.001$ vs. control group; $^{\#}P < 0.05$, $^{\#\#}P < 0.01$, $^{\#\#\#}P < 0.001$ vs. PhIP alone group; $^{\&\&}P < 0.01$, $^{\&\&\&}P < 0.001$ vs. PhIP + 5 μM SFN group; ns: not significant. Scale bars = 50 μm in **H**.

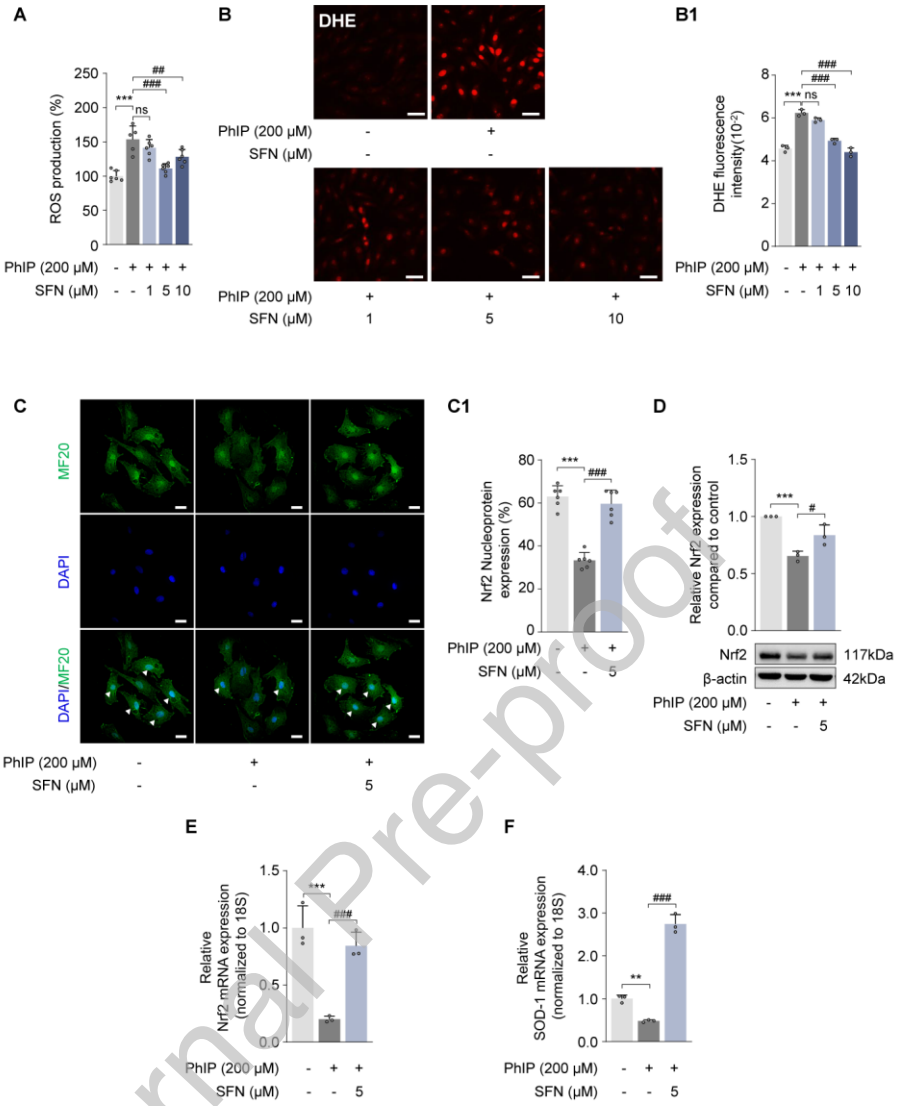

Fig. 3. Assessing the levels of oxidative stress in H9c2 cells following the PhIP treatment alone or in combination with SFN. (**A**) Representative data from flow cytometry in H9c2 cells in absence or presence of 200 μM PhIP and various concentrations of SFN (0, 1, 5 and 10 μM). Bar chart shows the comparisons of ROS production among the above groups. (**B-B1**) Representative images of dihydroethidium (DHE)-stained H9c2 cells in absence or presence of 200 μM PhIP and various concentrations of SFN (**B**). Bar chart shows the comparisons of DHE fluorescence intensity among the above groups (**B1**). (**C-C1**) Representative images

of Nrf2 Immunofluorescent staining on the H9c2 cells in absence or presence of 200 μM PhIP and 5 μM SFN (**C**); the bar chart shows the comparisons of the percentages of nuclear Nrf2-positive cells from above groups (**C1**). (**D**) Western blot data show the Nrf2 expressions at protein level in H9c2 cells in absence or presence of 200 μM PhIP and 5 μM SFN and the corresponding fold changes relative to control. (**E**-**F**) Quantitative PCR data show the Nrf2 (**E**) and SOD-1 (**F**) relative expressions at mRNA level in H9c2 cells in absence or presence of 200 μM PhIP and 5 μM SFN. Data were mean ± SD. n = 3 (**B**, **D**, **E**, **F**), n=6 (**C**), or n > 5 (**A**). $^{**}P < 0.01$, $^{***}P < 0.001$ *vs.* control group; $^{\#}P < 0.05$, $^{\#\#}P < 0.01$, $^{\#\#\#}P < 0.001$ *vs.* PhIP alone group; ns: not significant. Scale bars = 50 μm in **B**, or 20 μm in **C**.

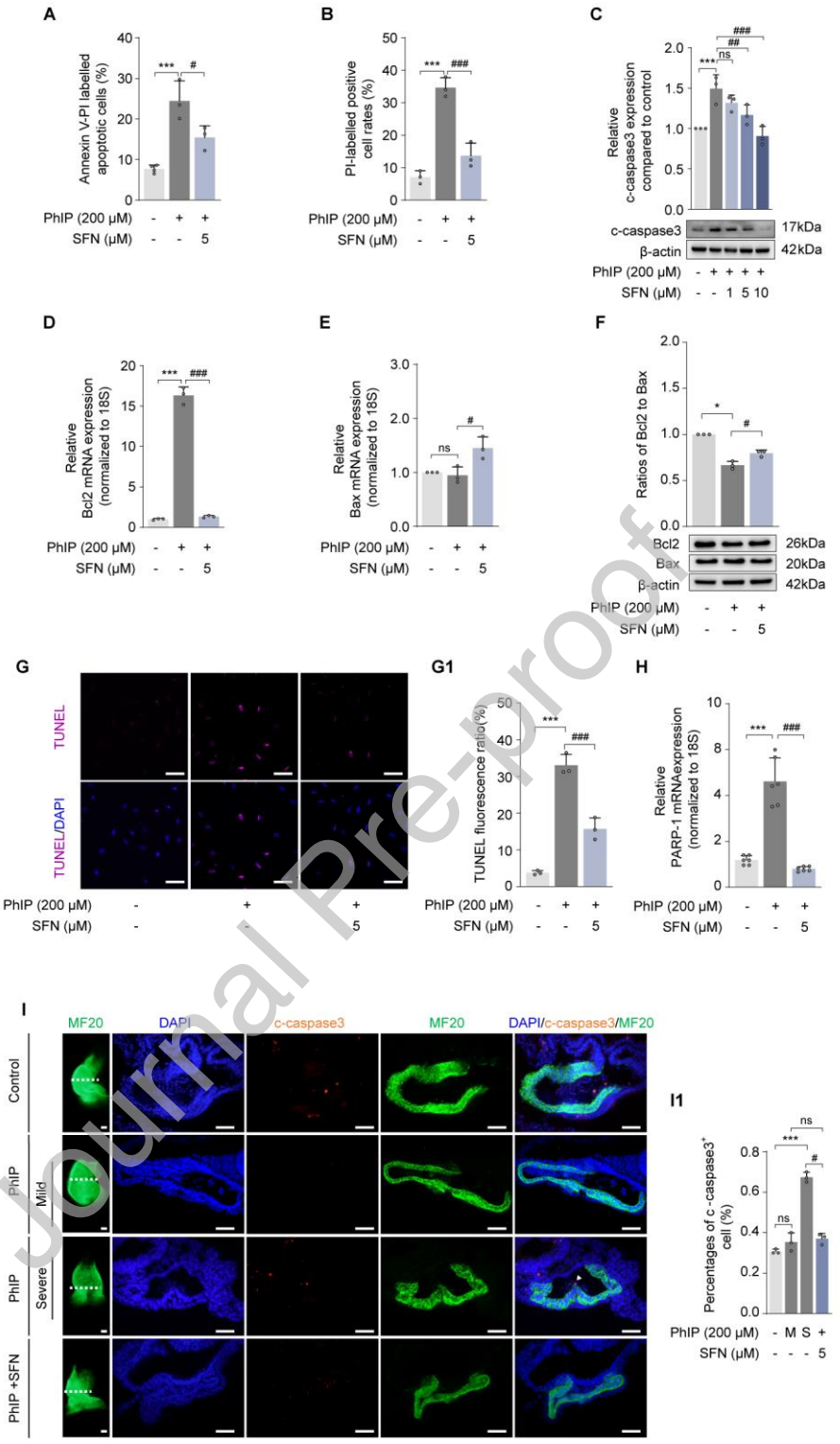

Fig. 4. Assessing the apoptosis in H9c2 cells and developing heart tubes following the PhIP treatment alone or in combination with SFN. (**A-B**) Bart charts show the percentages of Annexin V-PI labelled apoptotic cells (**A**), and PI-labelled positive

cells (**B**) in H9c2 cells in absence or presence of 200 μM PhIP and 5 μM SFN. (**C**) Western blot data show the c-caspase3 expressions at protein level in H9c2 cells in absence or presence of 200 μM PhIP and various concentrations of SFN. (**D-E**) Quantitative PCR data show the Bcl2 (**D**) and Bax (**E**) relative expressions at mRNA level in H9c2 cells in absence or presence of 200 μM PhIP and 5 μM SFN. (**F**) Western blot data show the Bcl-2/Bax ratio at protein level in H9c2 cells in absence or presence of 200 μM PhIP and 5 μM SFN. (**G-G1**) Representative images of TUNEL staining on the H9c2 cells in absence or presence of 200 μM PhIP and 5 μM SFN (**G**); the bar chart shows the comparisons of the percentages of TUNEL-positive cells from above groups (**G1**). (**H**) Quantitative PCR data show the PARP-1 relative expressions at mRNA level in H9c2 cells in absence or presence of 200 μM PhIP and 5 μM SFN. (**I-I1**) Representative images of the embryonic heart tubes (MF20 or c-caspase3 immunofluorescent staining) from control group, 200 μM PhIP alone group that caused mild or severe abnormality on heart tube phenotype, and 200 μM PhIP + 5 μM SFN group, as well as the cross sections of heart tubes at the leveled indicated by white dotted lines (**I**). Bar chart showing the percentages of c-caspase3 positive cells from the above-mentioned groups. Abbreviation: M, mild abnormality; S, severe abnormality (**I1**). Data were mean ± SD. n = 3 (**A-G**, **I**) or n=6 (**H**). $^{*}P < 0.05$, $^{**}P < 0.01$, $^{***}P < 0.001$ *vs.* control group; $^{\#}P < 0.05$, $^{\#\#}P < 0.05$, $^{\#\#\#}P < 0.001$ *vs.* PhIP alone group; ns: not significant. Scale bars = 50 μm in **G**, **I**.

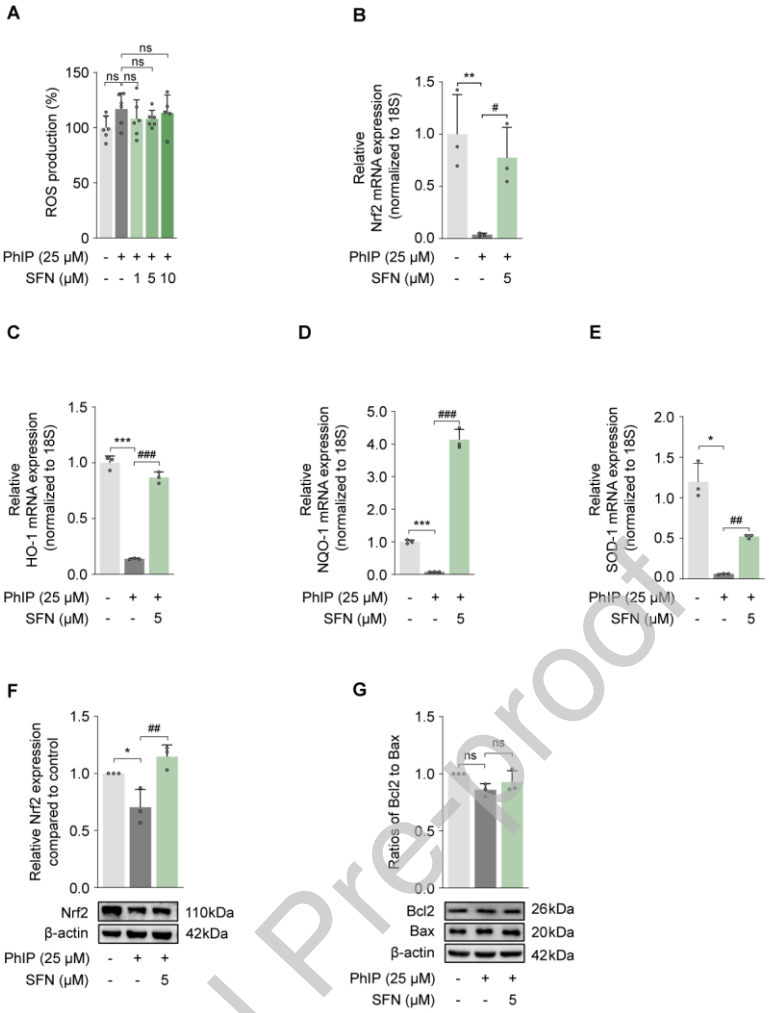

Fig. 5. Assessing the levels of oxidative stress in H9c2 cells following the low concentrations of PhIP treatment alone or in combination with SFN. (**A**) Representative flow cytometry in H9c2 cells in absence or presence of 25 μM PhIP and various concentrations of SFN (0, 1, 5 and 10 μM). Bar chart shows the comparisons of ROS production among the above groups. (**B-E**) Quantitative PCR data show the Nrf2 (**B**), HO-1 (**C**), NQO-1 (**D**) and SOD-1 (**E**) relative expressions at mRNA level in H9c2 cells in absence or presence of 25 μM PhIP and 5 μM SFN. (**F**) Western blot data show the Nrf2 expression at protein level in H9c2 cells in absence or presence of 25 μM PhIP and 5 μM SFN and the corresponding fold changes relative to control. (**G**) Western blot data show the Bcl2 and Bax expressions at

protein level in H9c2 cells in absence or presence of 25 μM PhIP and 5 μM SFN. Bar charts show the corresponding ratios of Bcl2 to Bax. Data were mean ± SD. n >5 (**A**), n = 3 (**B**-**G**). $^{*}P < 0.05$, $^{**}P < 0.01$, $^{***}P < 0.001$ *vs.* control group; $^{\#}P < 0.05$, $^{\#\#}P < 0.01$, $^{\#\#\#}P < 0.001$ *vs.* PhIP alone group; ns: not significant.

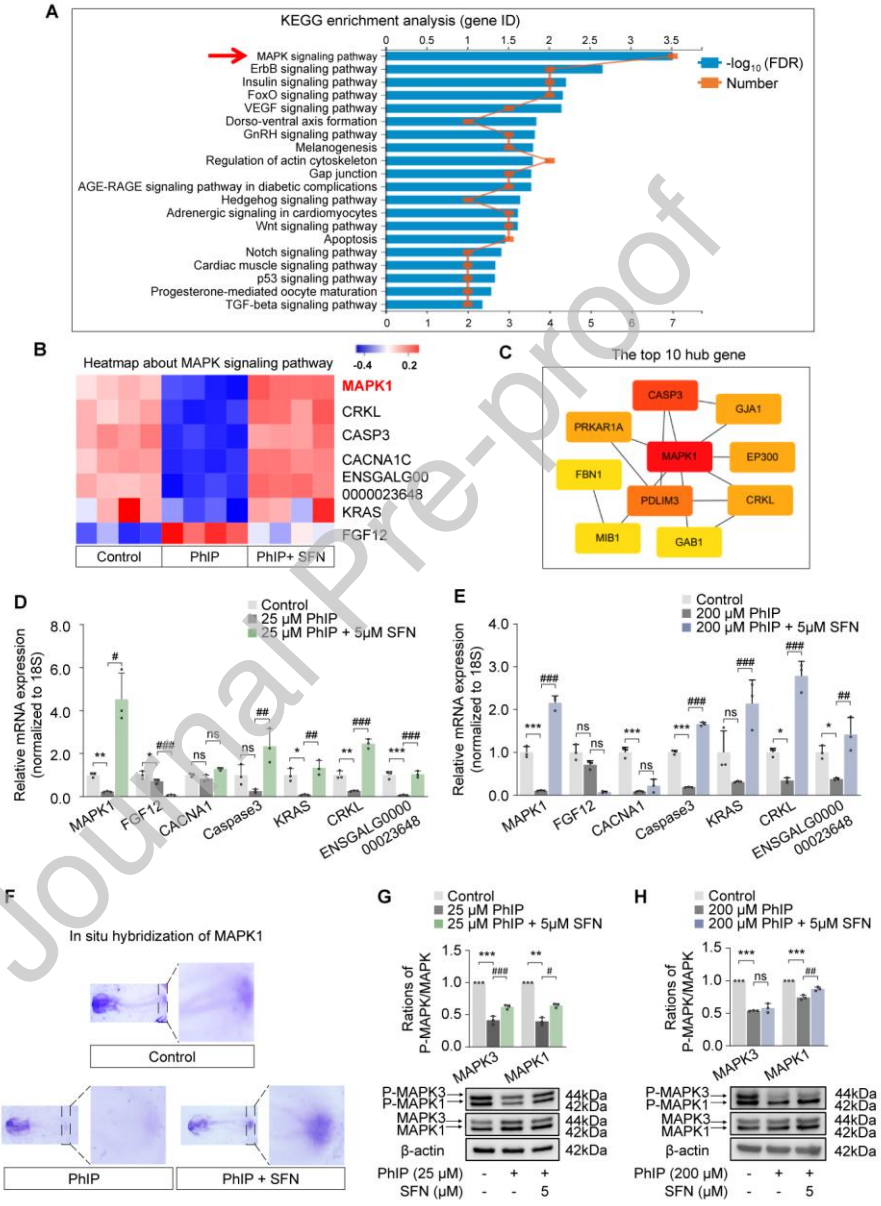

Fig. 6. Screening the key signaling pathway involved in the generation of phenotypes following the PhIP treatment alone or in combination with SFN.

(**A**-**C**) From the bioinformatic analysis of RNA-seq data, KEGG enrichment analyses

(**A**) and heatmap (**B**) revealed the most upregulated signaling pathways in 200 μM PhIP + 5 μM SFN group compared to control and PhIP alone groups, and the corresponding top hub genes were illustrated (**C**). (**D-E**) Quantitative PCR data show the relative expressions of a number of above-mentioned genes at mRNA level in H9c2 cells in absence or presence of 25 μM PhIP (**D**) or 200 μM PhIP (**E**) and 5 μM SFN. (**F**) Representative images of MAPK1 *in situ* hybridization in whole-mount chicken embryos from control, 200 μM PhIP alone and 200 μM PhIP + 5 μM SFN groups. (**G-H**) Western blot data show the P-MAPK1, P-MAPK3, MAPK1 and MAPK3 expressions at protein level in H9c2 cells in absence or presence of 25 μM PhIP (**G**) or 200 μM PhIP (**H**) and 5 μM SFN. Bar charts show the corresponding ratios of P-MAPK1 to MAPK1, and P-MAPK3 to MAPK3. Data were mean ± SD. n = 3 (**A, D-H**). $^{*}P < 0.05$, $^{**}P < 0.01$, $^{***}P < 0.001$ *vs.* control group; $^{\#}P < 0.05$, $^{\#\#}P < 0.01$, $^{\#\#\#}P < 0.001$ *vs.* PhIP alone group; ns: not significant. Scale bars = 50 μm in **F**.

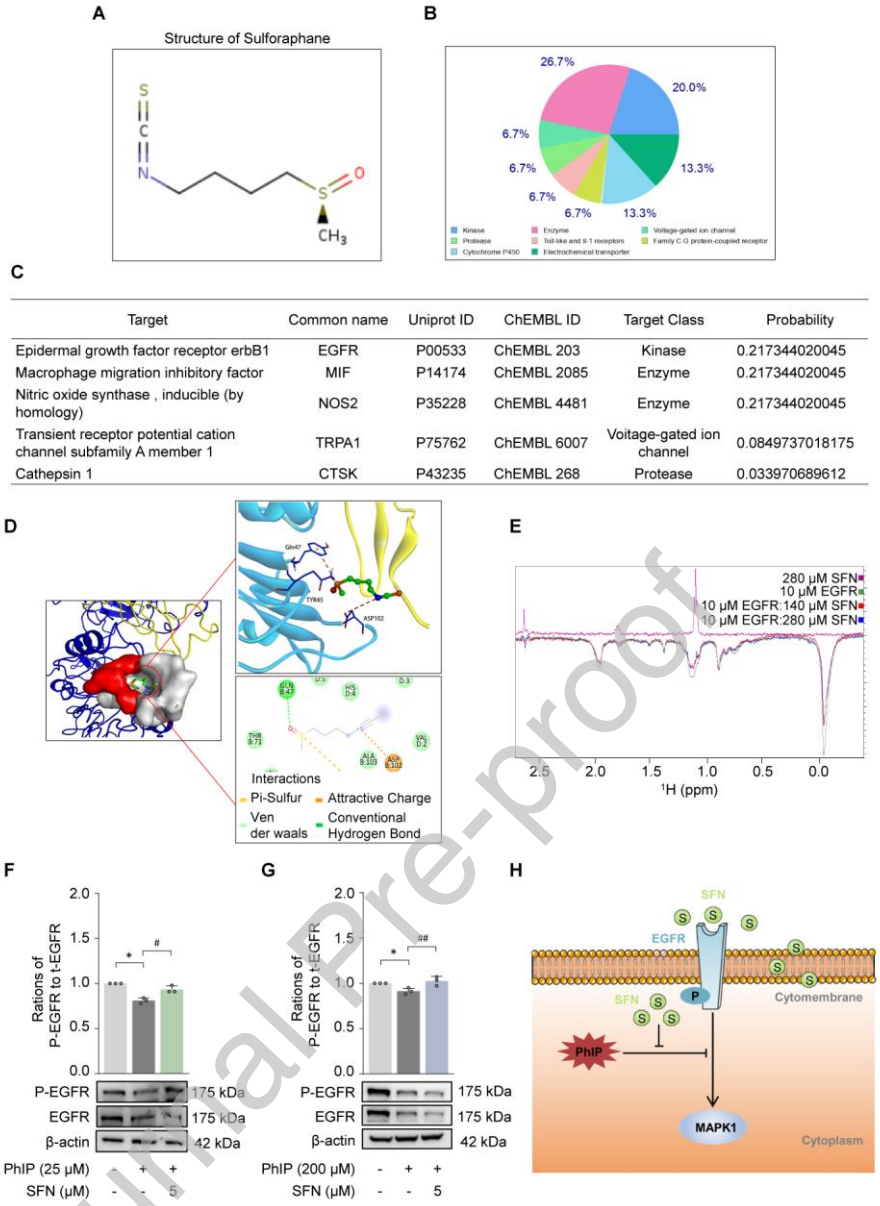

Fig. 7. Determining the molecular docking between SFN and EGFR signaling. (**A**) The two-dimensional structure of SFN according to SwissTargetPrediction. (**B**) Pie chart shows the category of SFN-regulated targets based on SwissTargetPrediction. (**C**) The table shows the information about the predicted most probable targets for SFN. (**D**) The proposed three- and two-dimension binding models of the interaction between SFN and EGFR derived from Open-Source PyMOL and Discovery Studio visualizer software. In the three-dimension interaction, EGFR is presented by carton, SFN is presented by ball-stick, and the binding residues are presented by stick. (**E**)

WaterLOGSY spectra show interaction between EGFR and SFN. Spectra were obtained by application of WaterLOGSY pulse cascade. SFN alone was phased positively (purple), and EGFR alone was phased negatively (green). Upon protein-ligand binding between EGFR and SFN, the sign of ^{1}H signals of SFN (e.g., ~2.63 ppm and ~1.79 ppm) are flipped negative (red and blue). (**F**, **G**) Western blot data show the P-EGFR/EGFR ratio in H9c2 cells in absence or presence of 25 μM PhIP (**F**) or 200μM PhIP (**G**) and 5 μM SFN. Bar charts show the corresponding ratios of P-EGFR to EGFR. (**H**) Schematic illustration of SFN/EGFR/MAPK1 signaling pathway against carcinogenic PhIP. Data were mean ± SD. n = 3 (**F**, **G**). $^{*}P < 0.05$ *vs.* control group; $^{\#}P < 0.05$ *vs.* PhIP alone group; ns: not significant.

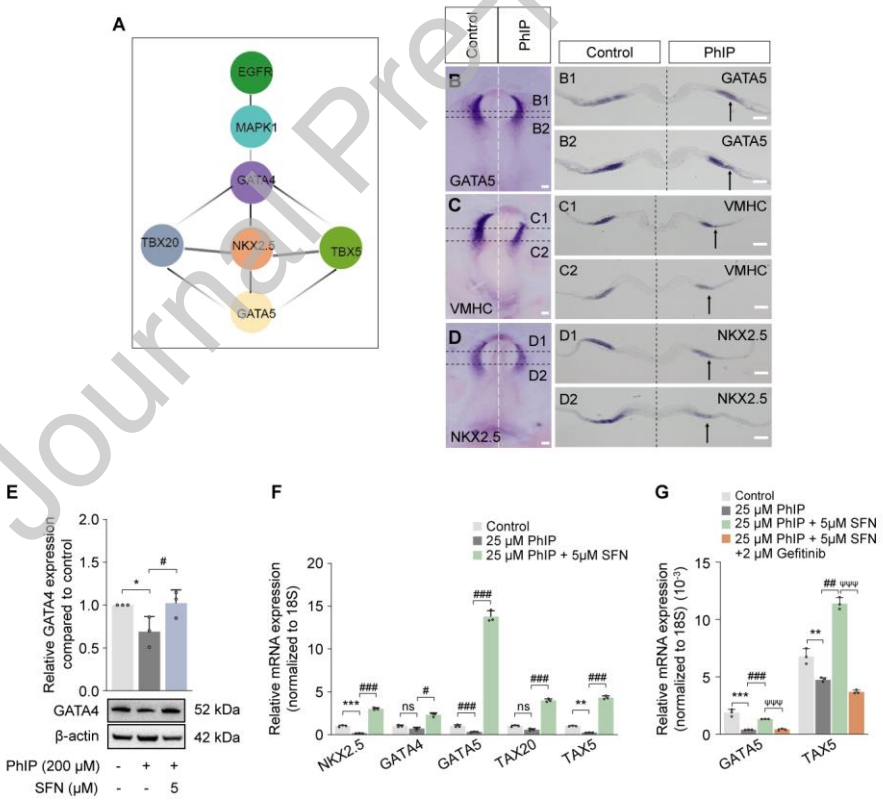

Fig. 8. Assessing the expressions of key genes involved in cardiogenesis following the PhIP treatment alone or in combination of SFN. (**A**) Schematic illustration of

String: functional enrichment analysis of protein-protein interaction network. (**B-D, B1-D1, B2-D2**) Representative images of GATA5 (**B**), VMHC (**C**) and NKX2.5 (**D**) *in situ* hybridization in whole-mount chicken embryos, which were exposed to 200 μM PhIP unilaterally (the right side of the chicken embryos), as well as the corresponding cross sections at the levels indicated by the dotted lines in **B-D** (**B1-D1, B2-D2**). (**E**) Western blot data show the GATA4 expression at protein level in H9c2 cells in absence or presence of 200 μM PhIP and 5 μM SFN. (**F**) Quantitative PCR data show the relative expressions of a number of key genes involved in cardiogenesis at mRNA level in H9c2 cells in absence or presence of 25 μM PhIP and 5 μM SFN. (**G**) Quantitative PCR data show the relative expressions of key genes involved in cardiogenesis at mRNA level in H9c2 cells in absence or presence of 25 μM PhIP and 5 μM SFN or 5 μM SFN + 2 μM gefitinib. Data were mean ± SD. n = 3 (**B-G**). $^{*}P < 0.05$, $^{**}P < 0.01$, $^{***}P < 0.001$ *vs.* control group; $^{\#}P < 0.05$, $^{\#\#}P < 0.01$, $^{\#\#\#}P < 0.001$ *vs.* PhIP alone group; $^{\Psi\Psi\Psi}P < 0.001$ *vs.* PhIP + SFN alone group. ns: not significant. Scale bars = 50 μm in **B-D**, **B1-D1**, **B2-D2**.

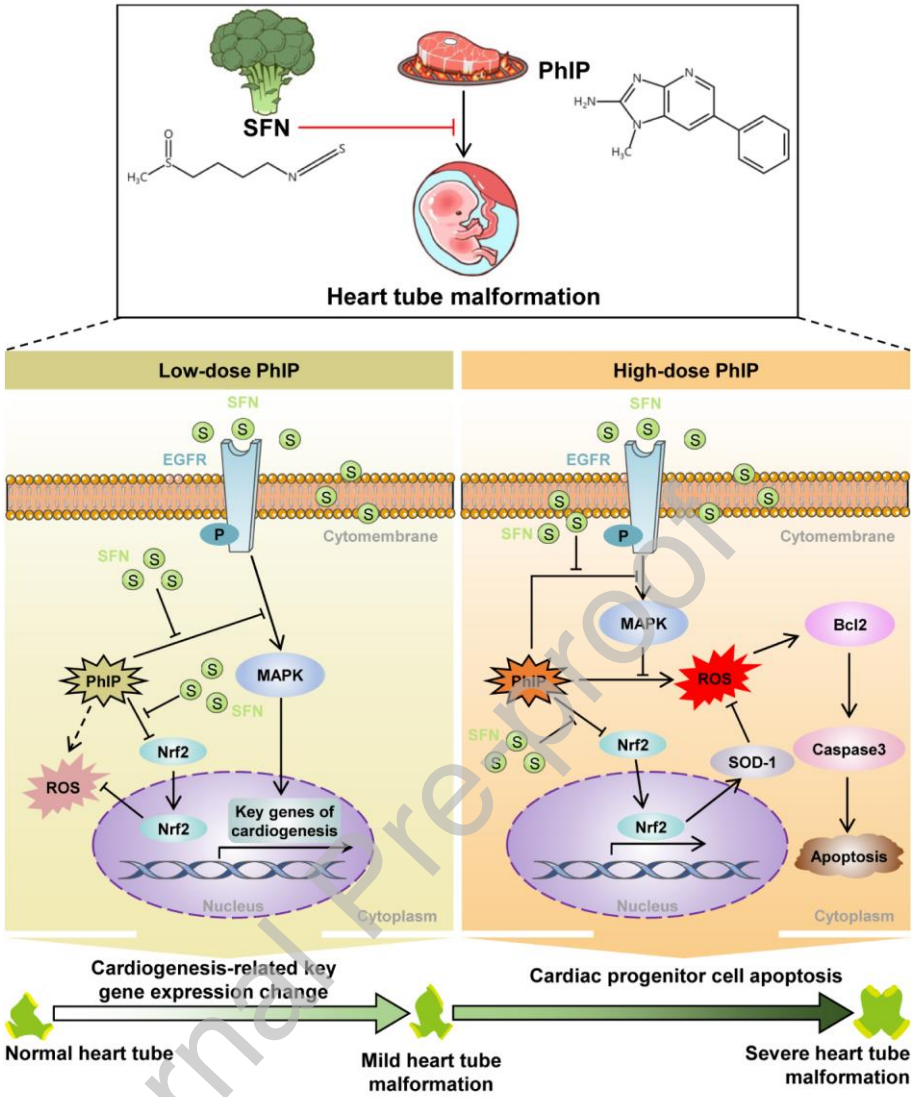

Fig. 9 Proposed mechanism of how sulforaphane-rescued heart tube malformation induced by various concentrations of PhIP exposure.

Graphical abstract

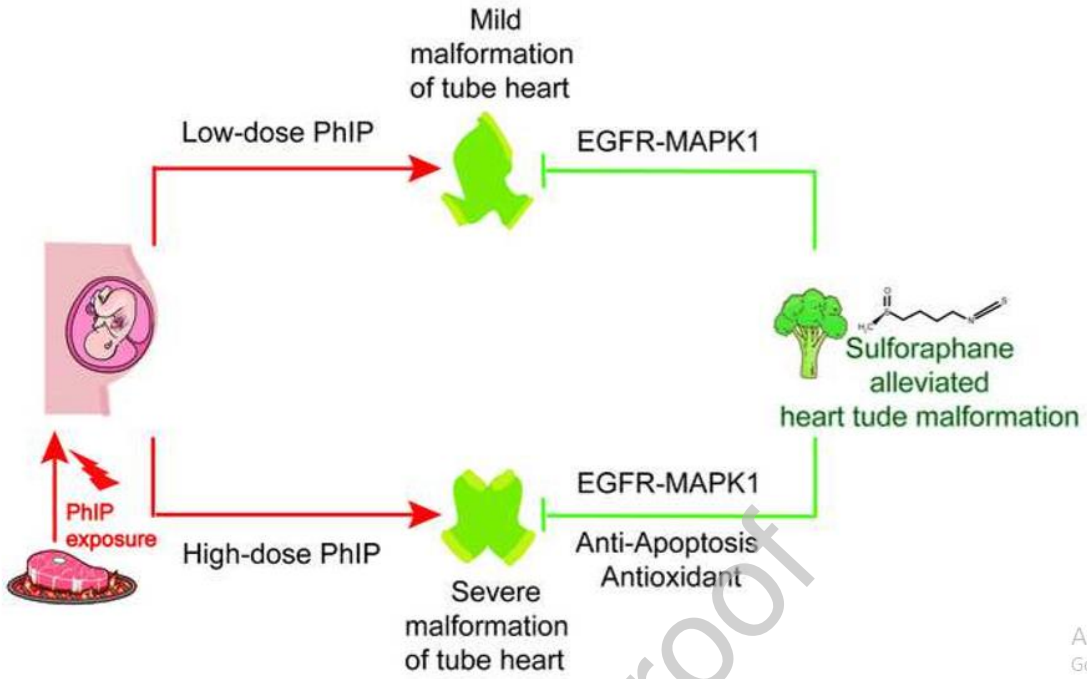

Declaration of Competing Interests

The authors report no conflict of interest.